PROCEEDINGS OF SCIENCE

$X_{\max}$ reconstruction based on radio detection of air showers

S. Buitink[*1], **A. Corstanje**[2], **J.E. Enriquez**[2], **H. Falcke**[2,3,4], **J.R. Hörandel**[2,3], **T. Huege**[5], **A. Nelles**[2,6], **J.P. Rachen**[2], **L. Rossetto**[2], **P. Schellart**[2], **O. Scholten**[7,8], **S. ter Veen**[2,4], **S. Thoudam**[2], **T.N.G. Trinh**[7]

1 *Astrophysical Institute, Vrije Universiteit Brussel, Pleinlaan 2, 1050 Brussels, Belgium*
2 *Department of Astrophysics/IMAPP, Radboud University Nijmegen, P.O. Box 9010, 6500 GL Nijmegen, The Netherlands*
3 *NIKHEF, Science Park Amsterdam, 1098 XG Amsterdam, The Netherlands*
4 *Netherlands Institute of Radio Astronomy (ASTRON), Postbus 2, 7990 AA Dwingeloo, The Netherlands*
5 *IKP, Karlsruhe Institute of Technology (KIT), Postfach 3640, 76021 Karlsruhe, Germany*
6 *Now at: Department of Physics and Astronomy, University of California Irvine, Irvine, CA 92697-4575, USA*
7 *KVI-CART, University Groningen, P.O. Box 72, 9700 AB Groningen, The Netherlands*
8 *Interuniversity Institute for High-Energy, Vrije Universiteit Brussel, Pleinlaan 2, 1050 Brussels, Belgium*
E-mail: Stijn.Buitink@vub.ac.be

The radio emission from air showers is used to accurately reconstruct the depth of the shower maximum ($X_{\max}$). We present a method based on using the full two-dimensional radiation profile as observed on the ground. While the density of shower particles reaching the ground is usually described with a 1D lateral distribution function, the intensity of the radio pulse is a complex function of observer position with respect to the shower axis. The CoREAS code simulates these complicated patterns to very high precision. When the antenna density is sufficiently high, like for example in the LOFAR core, the 2D approach leads to a resolution on $X_{\max}$ of < 20 g/cm2. This is the same level of accuracy that is achieved with fluorescence detection.

The 34th International Cosmic Ray Conference,
30 July- 6 August, 2015
The Hague, The Netherlands

*Speaker.

PoS(ICRC2015)369

1. Air shower detection with LOFAR

The cosmic ray mass composition contains important information about the nature of cosmic ray sources. In particular, mass measurements in the region between the knee and the ankle can be used to study the transition from a Galactic to extragalactic origin. It is yet unknown at what energy this transition occurs, and what the correct explanation is for the various features in the all-particle spectrum [1].

The cosmic-ray mass composition can be inferred from either the electron-to-muon ratio of the shower particles reaching the ground, or the atmospheric depth of the shower maximum $X_{\max}$. The well-established technique of fluorescence detection, used amongst others by the Pierre Auger Observatory [2] and the Telescope Array [3], is used above $10^{17.8}$ eV at a precision of ~ 20 g/cm^2. At lower energies, arrays such as Tunka [4] and Yakutsk [5], use non-imaging Cherenkov detectors, which are less precise. Both techniques suffer from the fact that they require dark night, limiting the duty cycle to $\sim 15\%$ [6].

Radio detection of air shower offers an alternative method of measuring $X_{\max}$, and has seen a rapid development in the last decade [7]. The first successful detections of air shower pulses took place in the 1960s [8], but it was not until this century that detection equipment became sophisticated enough to record the pulses with enough precision to make detailed study of the radiation mechanism [9]. A second generation of experiments, spearheaded by LOPES [10] and CODALEMA [11], has demonstrated the main features of the radio emission, and its potential to provide $X_{\max}$ measurements [12].

Today, LOFAR [13] produces the most detailed air shower radio data ever, by using the dense core region, or *superterp*, where 384 antennas are located within a circle of 320 m diameter. A particle array, LORA [14], has been installed in the core and is used for triggering and reconstruction. Each antenna contains a ring buffer which is read-out in case of a trigger. The full waveform is stored for offline analysis [15].

The high antenna density of LOFAR has allowed studies of unprecedented detail into various characteristics of the radio emission: the shape of the wavefront [16], the signal polarization [17], the frequency dependence [18], and the influence of strong electric fields in thunderstorms [19]. Here, we focus on the distribution of the radio power as observed on the ground. The distribution function is not rotationally symmetric, so high-resolution reconstructions require a two-dimensional treatment of the power distribution profile. It has been demonstrated that this approach leads to a resolution on $X_{\max}$ below 20 g/cm^2 for densely populated arrays like LOFAR [20]. This is comparable to fluorescence detection, but the radio detection technique has a duty cycle of nearly 100% [21].

2. CoREAS simulations

The radio emission from air showers can be understood as superposition of two radiation mechanisms. The dominant contribution is geomagnetic radiation [22, 9, 23], caused by interaction of shower electrons and positrons with the Earth's magnetic field. It is linearly polarized in the direction of the Lorenz force, or $\mathbf{v} \times \mathbf{B}$, where $\mathbf{v}$ is the velocity of the shower front, and $\mathbf{B}$ is the geomagnetic field. A secondary component is due to the accumulation of a charge excess in the

shower front [24, 25]. Charge excess radiation typically contributes $5-20\%$ of the total radiation [17, 26] and its polarization vector point radially away from the shower axis.

The total observed radiation field is the vector sum of these two contributions. Depending on the observer position relative to the shower axis, the two components can add constructively or destructively, leading to an asymmetrical, bean-shaped power distribution profile. The maximum and minimum interference occurs at the $\mathbf{v}\times\mathbf{B}$ axis, which therefore provides a natural coordinate system for presenting the data (see Fig. 1).

The CoREAS code [27] simulates the radio emission of air showers and is available as a plug-in of CORSIKA [28]. It adds the individual radiation contributions of all shower electrons and positrons, making use of the endpoint formalism [29]. This can be regarded as a direct application of the Maxwell equations to the charge distribution of the shower, and therefore this approach does not make any implicit assumptions on the radiation mechanism. Nonetheless, the simulation outcomes can be understood in terms of geomagnetic and charge excess radiation [30].

We use CORSIKA 7.400, with hadronic interaction models FLUKA 2011.2b [31] and QGSJETII.04 [32]. Thinning is applied at a level of 10^{-6} with optimised weight limitation [33]. The response of the LORA detectors is simulated with GEANT4 [34].

3. Shower reconstruction

We have developed a reconstruction method that is based on a simultaneous fit of the two-dimensional radio power profile and the lateral distribution function of the particle density. The method is applied to all showers that were recorded by antennas in at least four *stations*. Stations are dense groups of antennas, of which 48 are actively recording simultaneously. Since one station only samples a small part of the radio footprint multiple stations are needed for a good reconstruction. This means the showers in our event sample are recorded by ~ 200 antennas or more.

For each shower we produce a dedicated set of CORSIKA simulations, corresponding to its arrival direction and an energy estimate based on a fast parametrization [35, 36]. To cover a large range of possible $X_{\max}$ values we produce 50 proton showers and 25 iron showers.

CoREAS outputs the radiation field for specific locations on the ground. Since the core position is a free parameter in our fit, we do not know the antenna position with respect to the shower axis beforehand. Instead, we calculate the radiation for a star-shaped pattern of antenna positions. For each virtual antenna we calculate the total received power in a 55 ns window. From interpolation of these values we produce a two-dimensional power profile [20].

The power profiles are fitted to the data together with the particle data, by minimising:

$$\chi^2 = \sum_{\text{antennas}} \left(\frac{P_{\text{ant}} - f_r^2 P_{\text{sim}}(x_{\text{ant}} - x_0, y_{\text{ant}} - y_0)}{\sigma_{\text{ant}}} \right)^2 + \sum_{\substack{\text{particle}\\ \text{detectors}}} \left(\frac{d_{\text{det}} - f_p d_{\text{sim}}(x_{\text{det}} - x_0, y_{\text{det}} - y_0)}{\sigma_{\text{det}}} \right)^2, \tag{3.1}$$

where P_{ant} is the measured power integrated over a 55 ns window at an antenna at location $(x_{\text{ant}}, y_{\text{ant}})$ with noise level σ_{ant}, P_{sim} is the simulated power, d_{det} is the deposited energy as measured by a LORA detector at location $(x_{\text{det}}, y_{\text{det}})$ with noise σ_{det}, and d_{sim} is the simulated deposited energy.

The fit contains four free parameters, two of which describe the location of the shower axis (x_0, y_0). A scaling parameter f_p for the particle lateral distribution function is needed to correct the energy scale, while a scaling parameter for the radio power f_r^2 is needed because the antennas do not yet have an absolute calibration. When f_p deviates from unity, the reconstructed energy is different than the simulated energy. When the deviation is large, a new set of simulation is produced at the reconstructed energy. The procedure is repeated until the energy is consistent within the resolution of 32%.

Two example showers are shown in Fig. 1. The left panels correspond to an inclined shower (55 degrees zenith angle) producing a large footprint. The shower in the right panels has a smaller inclination of 26 degrees zenith angle. The circles indicate the antenna positions (projected into the shower plane) and their colors represent the measured power. The background color map is the power profile as simulated by CoREAS. For a good fit, the circle colors have to blend into the background.

The panels in the middle row show the measured and simulated power for each antenna as a function of distance to the shower axis. Clearly, the data could not have been fit with a single-valued lateral distribution function. The shapes observed in these plots depend on the antenna positions (indeed a station ring structure can be seen in the right plot) and are completely different for each shower.

The plots in the top two rows show the best fitting simulation out of the complete set of CORSIKA showers that was produced for that particular observation. The bottom row shows the reduced χ^2 of the fit (Eqn. 3.1) as a function of simulated $X_{\max}$. The points follow a curve that has a clearly defined minimum. We reconstruct $X_{\max}$ by fitting a parabola to a selection of best-performing fits.

The depth of the shower maximum is only one of features in the shower development that is different in each simulation. These plots demonstrate that it is by far the most important parameter in determining the quality-of-fit. Other fluctuations cause the "jitter" of the data points around the curve.

The uncertainty on the reconstructed $X_{\max}$ is found with a Monte Carlo study and depends on the shower geometry. Figure 2 shows a distribution of the uncertainty for 118 showers. The mean value is ~ 15 g/cm^2.

All simulations were produced with the same atmosphere in CORSIKA. The observed radio pattern on the ground in fact depends on the altitude h_X of $X_{\max}$. We make a correction by constructing a local, up-to-date atmospheric density profile and evaluating which slant depth corresponds to the reconstructed h_X. We use a method developed by the Auger collaboration [37] that makes use of atmospheric information that is retrieved from the Global Data Assimilation System (GDAS) [38]. At Auger it was found that after correction, the statistical uncertainty due to the changing atmosphere is very small (~ 1 g/cm^2). We assume that the situation in the Netherlands will not be worse, given the higher density of weather station providing GDAS with data, and the unspectacular geography.

The uncertainty in the angular reconstruction translates into an additional uncertainty on $X_{\max}$, since different zenith angles correspond to different total slant depths. Currently we use a plane wave approximation for reconstruction the arrival direction, yielding a resolution of $\sim 1^\circ$ in zenith

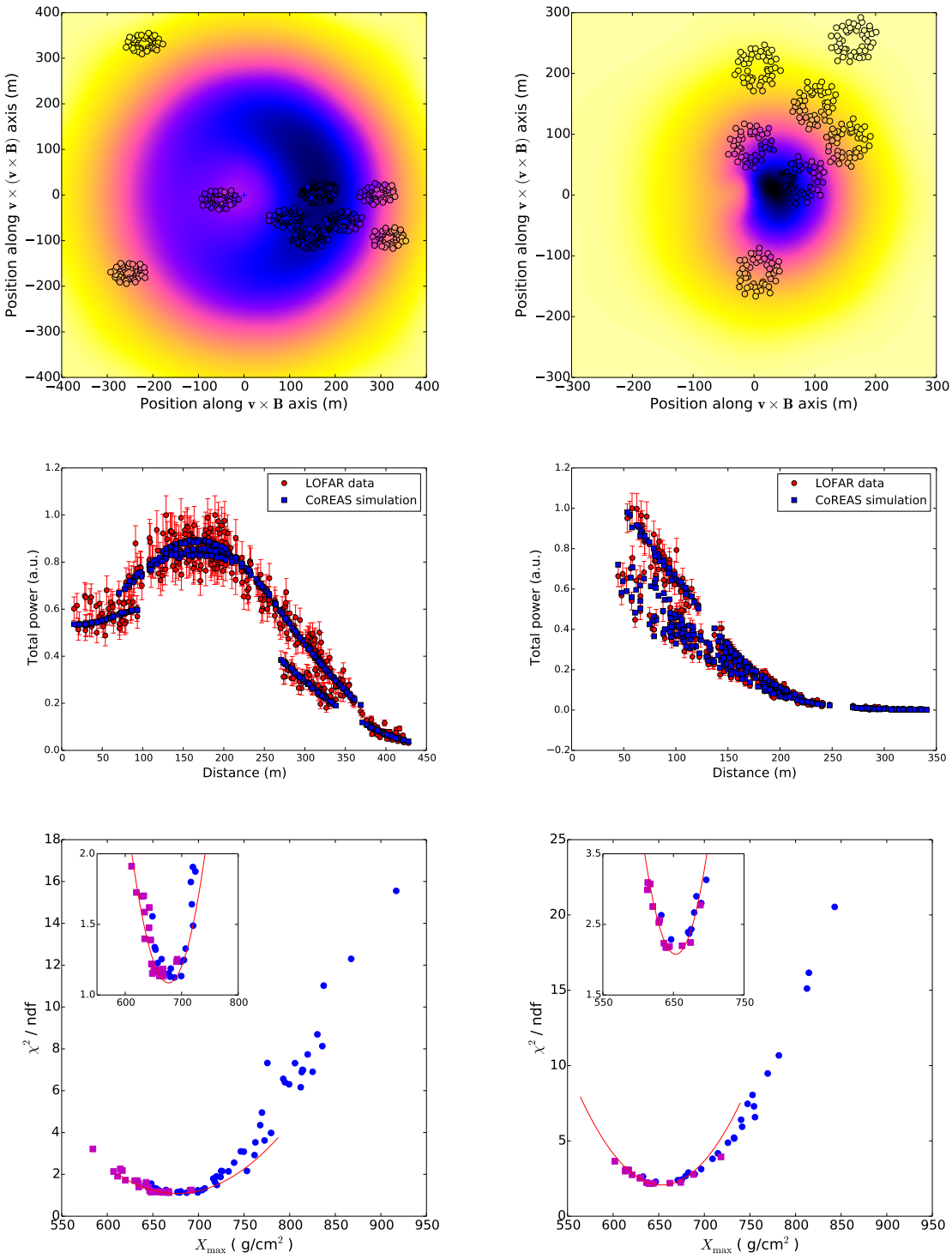

Figure 1: Two-dimensional radio air shower reconstructions. The measured power for two different showers (left/right) is fitted to a simulated radio map (top panels). The one-dimensional lateral distribution functions (middle panels) are not single-valued functions of distance to the shower axis. The reconstructed $X_{\max}$is found by plotting the quality-of-fit for all simulations (bottom panels).

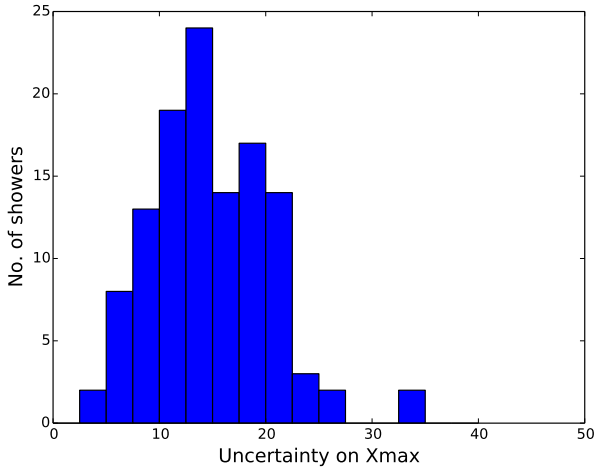

Figure 2: Distribution of uncertainty on $X_{\max}$ for 118 reconstructed showers. The mean value is ~ 15 g/cm^2.

or ~ 2 g/cm^2 in $X_{\max}$. The resolution can be improved by an order of magnitude by using a more realistic, hyperbolic geometry of the wave front [16].

4. Model dependence

Hadronic interaction models Several codes exist to simulate the interaction of high-energy hadrons. At lower energies the models are in agreement with accelerator data, but above the LHC energy the prediction start to diverge. For example, in the LOFAR energy range, around 10^{17} eV, the mean $X_{\max}$ as predicted by QGSJETII.04 and EPOS-LHC [40] differ by 10-20 g/cm^2. This complicates the interpretation of the measured $X_{\max}$ distribution in terms of mass composition, but does not necessarily lead to a systematic uncertainty in the reconstruction of $X_{\max}$ itself. For example, for the fluorescence detection technique, the measurements of $X_{\max}$ do not depend on hadronic interaction models at all, because it is a geometrical measurement. For radio detection the situation is slightly different. Although it is also in principle a geometrical measurement, the reconstruction technique described here uses sets of CORSIKA simulations for which a hadronic model must be chosen. Different models may produce longitudinal profiles that are different in shape, and therefore create different radiation pattern on the ground. We have found a systematic offset of ~ 4 g/cm^2 when we reconstruct EPOS showers using a sample of QGSJETII showers [20].

Radio simulation codes In contrast to hadronic interactions, the radiation from charged particles can be derived from first principles. Therefore, the challenge of correctly calculating the radio emission is mainly to make sure that all contributions are taken into account. This is solved rigorously by microscopic codes such as CoREAS and ZHAireS [39], in which the radiation fields of all shower electrons and positrons are added together. These two codes, that were developed completely independently, now produce very similar results [30]. A remaining discrepancy between the two codes is an offset in the absolute scale, to which the method described here is insensitive.

5. Conclusion

We have demonstrated an accurate technique for the reconstruction of $X_{\max}$ based on radio measurements. The high precision is achieved by making use of two-dimensional radio power profiles, and a dense sampling of that profile with hundreds of antennas. The excellent agreement between data and simulation demonstrates that the radio emission is now well-understood. LOFAR operates in the $10^{16.5} - 10^{17.5}$ eV range and can thus be used to study cosmic-ray mass composition below the ankle.

The extreme antenna density of LOFAR has been very useful for detailed verification of radio emission simulations, but is not needed for reconstruction. The Auger Engineering Radio Area (AERA) [26] explores the optimal antenna spacing that balances cost and accuracy. Observations at this site can also be used for a direct comparison between radio and fluorescence measurements on a per-shower basis.

The low-frequency core of the SKA will have $\sim 60,000$ antennas in an area of ~ 1 km^2. The antennas have a larger bandwidth and will be more evenly distributed than the LOFAR antennas that are grouped in circles. Therefore, the SKA can become an excellent site for high-resolution cosmic-ray mass composition studies [41].

6. Acknowledgement

The LOFAR cosmic ray key science project acknowledges funding from an Advanced Grant of the European Research Council (FP/2007-2013) / ERC Grant Agreement n. 227610. The project has also received funding from the European Research Council (ERC) under the European Union's Horizon 2020 research and innovation programme (grant agreement No 640130). We furthermore acknowledge financial support from FOM, (FOM-project 12PR304) and NWO (VENI grant 639-041-130). AN is supported by the DFG (research fellowship NE 2031/1-1).

LOFAR, the Low Frequency Array designed and constructed by ASTRON, has facilities in several countries, that are owned by various parties (each with their own funding sources), and that are collectively operated by the International LOFAR Telescope foundation under a joint scientific policy.

References

[1] K.-H. Kampert and M. Unger, M., Astropart. Phys. **35**, 660 (2012).

[2] A. Aab *et al.* [Pierre Auger collaboration], Phys. Rev. D **90**, 122006 (2014).

[3] R. U. Abbasi *et al.* [TA collaboration.], Astropart. Phys. **64**, 49 (2015).

[4] S. F. Berezhnev *et al.* [Tunka collaboration.], Proc. 32nd ICRC Beijing **209** (2011).

[5] S. Knurenko and A. Sabourov, A. [Yakutsk collaboration], Proc. XVI ISVHECRI (2010).

[6] J. Abraham *et al.* [Pierre Auger collaboration], Nucl. Instr. and Meth. in Phys. Res. A **620**, 227Đ251 (2010).

[7] T. Huege, Brazilian J. Phys. **44**, 520 (2014).

[8] H. R. Allan, Prog. Elem. Part. Cosm. Ray Phys. **10**, 171 (1971).

[9] H. Falcke and P. W. Gorham, Astropart. Phys. **19**, 477 (2003).

[10] H. Falcke *et al.*, Nature **435**, 313 (2005).

[11] A. Bellétoile *et al.* [CODALEMA collaboration], Astropart. Phys. **69**, 50 (2015).

[12] Apel, W. *et al.* [LOPES collaboration] Phys. Rev. D **90**, 062001 (2014).

[13] M. P. van Haarlem *et al.* [LOFAR collaboration], Astron. & Astrophys. **556**, A2 (2013).

[14] S. Thoudam *et al.*, [LOFAR collaboration], Nucl. Instr. and Meth. in Phys. Res. A **767**, 339 (2014).

[15] P. Schellart *et al.* [LOFAR collaboration], Astron. & Astrophys. **560**, A98 (2013).

[16] A. Corstanje *et al.* [LOFAR collaboration], Astropart. Phys. **61**, 22 (2015).

[17] P. Schellart *et al.* [LOFAR collaboration], J. Cosm. Astropart. Phys. **10**, 14 (2014).

[18] A. Nelles *et al.* [LOFAR collaboration], Astropart. Phys. **65**, 11 (2015).

[19] P. Schellart *et al.* [LOFAR collaboration], Phys. Rev. Lett. **114**, 165001 (2105).

[20] S. Buitink *et al.* [LOFAR collaboration], Phys. Rev. D **90**, 082003 (2014).

[21] S. Buitink *et al.* [LOPES collaboration], Astron. & Astrophys. **467**, 385 (2007).

[22] F. D. Kahn and I. Lerche, Roy. Soc. Lond. Proc. Ser. A, **289**, 206 (1966).

[23] K. Werner and O. Scholten, Astropart. Phys. **29**, 393 (2008).

[24] G. A. Askaryan, JETP **14** 441Ð443 (1962).

[25] K. D. de Vries, O. Scholten, and K. Werner, Astropart. Phys. **45**, 23 (2013).

[26] A. Aab *et al.* [Pierre Auger collaboration], Phys. Rev. D **89**, 2002 (2014).

[27] T. Huege, M. Ludwig, and C. James, AIP Conference Proceedings **1535**, 128-132 (2012).

[28] D. Heck, Report FZKA **6019** (1998).

[29] C. James, H. Falcke, T. Huege, and M. Ludwig, Phys. Rev. E **84**, 056602 (2011).

[30] T. Huege *et al.*, Nucl. Instr. and Meth. in Phys. Res. A **662**, 179 (2012).

[31] G. Battistoni *et al.* AIP Conf. Proc. **896**, 31 (2007).

[32] S. Ostapchenko, Nucl. Phys. B Proc. Suppl. **151**, 147 (2006).

[33] M. Kobal *et al.* [Pierre Auger collaboration], Astropart. Phys. **15**, 259 (2001).

[34] S. Agostinelli *et al.*, NIMPA **506**, 250 (2003).

[35] A. Nelles *et al.*, Astropart. Phys. **60**, 13 (2015).

[36] A. Nelles *et al.*, J. Cosm. Astropart. Phys. **5**, 18 (2015).

[37] P. Abreu *et al.* [Pierre Auger collaboration], Astropart. Phys. **35**, 591 (2012).

[38] NOAA Air Resources Laboratory (ARL), Global Data Assimilation System (GDAS1) Archive Information, Tech. rep. (2004).

[39] J. Alvarez-Muñiz *et al.*, Astropart. Phys. **35**, 325 (2012).

[40] T. Pierog and K. Werner, Nucl. Phys. B Proc. Suppl. **196**, 102 (2009).

[41] T. Huege *et al.*, Proceedings of Advancing Astrophysics with the Square Kilometre Array (AASKA14). 9 -13 June, 2014. Giardini Naxos, Italy. (id.148) [arXiv:1408.5288]